The formation of vortex streets

By FREDERICK H. ABERNATHY
AND RICHARD E. KRONAUER

Division of Engineering and Applied Physics, Harvard University,
Cambridge, Massachusetts

(Received 7 December 1961)

The formation of vortex streets in the wake of two-dimensional bluff bodies can be explained by considering the non-linear interaction of two infinite vortex sheets, initially a fixed distance, h, apart, in an inviscid incompressible fluid. The interaction of such sheets (represented in the calculation by rows of point-vortices) is examined in detail for various ratios of h to the wavelength, a, of the initial disturbance. The number and strength of the concentrated regions of vorticity formed in the interaction depend very strongly on h/a. The non-linear interaction of the two vortex sheets explains both the cancellation of vorticity and vortex-street broadening observed in the wakes of bluff bodies.

1. Introduction

Interest in the wakes in flow past bluff bodies has been evidenced since the early experiments of Strouhal in 1878 concerning 'aeolian tones' emanating from a wire moving through air; however, it was not until von Karman (1911) published his first paper on the theory of vortex streets that a widespread continuing research interest in vortex-street phenomena began. Goldstein (1938) has summarized most of the early research in this field. Theoretical studies were primarily concerned with elaborations of the stability analysis of alternate rows of point vortices, while experimental investigations were chiefly concerned with the frequency of the velocity fluctuations in the wake due to vortex streets.

Many of the important features of the flow near a bluff body and of the vortex street itself were elucidated by Fage & Johansen (1927, 1928). At Reynolds numbers large enough for a vortex street to develop in the wake of a bluff body, they found that the boundary layers separated from the upper and lower surface of the body and were convected downstream in the wake. These free vortex layers separated the outer flow (which was essentially potential flow) from the region of very low velocity which existed immediately behind the bluff body. Since the boundary layers separated at points on the body where the time-average speed in the external flow was U_s, considerably greater than the speed of the undisturbed stream, the rate at which vorticity was discharged from the body into each vortex layer was found experimentally to be $\frac{1}{2}U_s^2$.

With regard to the vortex street itself, Fage & Johansen (1927) reported that the ratio of the width of the street to the distance between adjacent vortices in the same row increased with the downstream distance behind the body. Near the

body the ratio was very nearly that predicted by Karman (1911), while far downstream the ratio had increased by about a factor of two. At the same time, using hot-wire anemometer techniques they attempted to measure the rate at which vorticity of a given sign was convected downstream in the form of large individual eddies in the vortex street. This quantity cannot be measured directly, and any estimation of the value involves assumptions about the distribution of vorticity within eddies as well as about the street geometry. Nevertheless their estimation that only 60 % of the vorticity discharged from the edges of a normal flat plate ended up in the large individual eddies appears reasonable. In spite of these and other important investigations the mechanism of the formation of the vortex street, downstream in the wake of a bluff body, from the free vortex layers discharged from the body has never been explained.

One might expect that photographic studies would explain the mechanism of the formation of the vortex street; however, this does not appear to be the case. Homann (1936) obtained excellent photographs of oil slicks on the free surface of water which show a vortex street forming behind a cylinder. The widening of the street with the distance downstream of the cylinder is clearly shown; still the mechanism of the street formation is obscure. More recently Lippisch (1958) has published a high-speed photograph of smoke trails showing strong interaction between the free vortex layers behind a cylinder; however, this too leaves most questions about the mechanism of the formation of vortex streets unanswered. The purpose of this paper is to explain the essential features of this mechanism of formation using a relatively simple flow model. It will be shown that the model accounts for wake widening and for cancellation of vorticity in the transition from free vortex layers to vortex streets.

2. The flow model

Ideally one would like to analyse mathematically the time history of perturbations in the steady flow of a viscous incompressible fluid past a two-dimensional bluff body; however, the steady solution has yet to be found. Since it is the unsteady problem which is of interest here, major simplifications of the flow model are needed.

Let us consider first the importance of viscosity in the formation of the vortex street. Viscosity is important for the formation of the vortex layers emanating from the bluff body; however, it is not clear that viscosity is essential to the formation of the vortex street provided the free vortex layers exist initially. Kovasznay (1949) and Roshko (1954*a*) have both observed that below a Reynolds number of 40 there is no vortex street formed in the wake of a circular cylinder; while in the Reynolds number range from 40 to 140 the vortex street is regular and stable. In the latter range of Reynolds number the Strouhal number (dimensionless frequency formed with the free stream velocity and the cylinder diameter) of the vortex street varies from 0·12 at the lower limit to about 0·185 at the upper limit. In the range of the Reynolds number from about 300 to about 100,000 the velocity fluctuations in the wake of a cylinder due to the vortex street are not regular, although a predominant frequency can be determined. The Strouhal number in this Reynolds number range is almost constant, varying from

about 0·20 at both ends of the range to 0·21 in between. This is the same Reynolds number range in which the drag coefficient for a cylinder is constant. In geometrically similar situations, an increasing Reynolds number implies a declining influence of viscous forces compared with inertia forces in the fluid. Since neither the drag coefficient nor the Strouhal number are functions of the Reynolds number over this considerable range, it would appear that viscosity cannot contribute significantly to the mechanism of vortex street formation.

It is true that the growth rate of infinitesimal disturbances in a single layer of vorticity bounded above and below by potential flow is influenced by the distribution of vorticity in the layer (the distribution representing the influence of vortex diffusion) provided the wavelength of the disturbance is of the same order of magnitude as the thickness of the sheet (Rayleigh 1894). Nevertheless, when the wavelength of the disturbance is large compared with the thickness of the sheet, the growth rate is independent of the distribution of the vorticity within the layer and is the same as the growth rate for a similar disturbance in a vortex sheet. Since the ratio of the distance between concentrated vortices in the same row of a vortex street to the thickness of the free vortex layers behind a bluff body is at least 25 (Fage & Johansen 1927), it would appear, on the basis of the initial growth rates of the predominant disturbances, that it is also reasonable to disregard the finite thickness of the free vortex layers and to idealize them as free vortex sheets.

Let us now examine the role of the bluff body in the formation of a vortex street. The flow over the body is responsible for the free vortex layers (which will be idealized as free vortex sheets); but given two parallel vortex sheets separated by some initial distance, is it necessary to have a solid body between them in order to form a vortex street? On the basis of the calculations to be presented in this paper the answer is definitely no. There is also experimental evidence which suggests that the body is not very important in the formation of the vortex street (excluding its role in the generation of the vortex layers). Fage & Johansen (1927, 1928) and Roshko (1954*b*) were able to form Strouhal numbers, which were found to be essentially the same for all two-dimensional bluff bodies, using only the distance between the vortex layers, the vortex-street frequency, and the characteristic velocity U_s. Therefore, it was decided that one should expect two initially parallel vortex sheets to interact to form a vortex street.

Focusing attention on a wavelength of the sheets as they are produced at some fixed location and following them as they are convected downstream, one would see the development of individual eddies in the vortex street. Provided the transition from sheet to street does not take place too abruptly, this development can be simulated by the growth in time of periodic disturbances in two infinitely long parallel sheets.

3. Linear analysis

Rayleigh (1894) initially investigated the transient response to small amplitude disturbances of two infinite, parallel vortex sheets for inviscid incompressible flow. He showed that such vortex sheets were unstable to perturbations of all wavelengths. Here we present the results of such an analysis (in a more general form than the authors have found elsewhere) which are needed for the non-linear

investigations of the next section. Rayleigh calculated the growth rate of symmetric, sinusoidal, vertical displacements in both vortex sheets. His results can be generalized to include perturbations in the strength of vorticity along the sheets in addition to vertical displacements of the sheets. The vortex sheets, subjected to a small but arbitrary initial disturbance, are sketched in figure 1.

Any arbitrary displacement of the elements of the sheets can be characterized by four independent functions of x. Two of these functions are associated with each sheet; they describe the horizontal and vertical displacements ξ and η

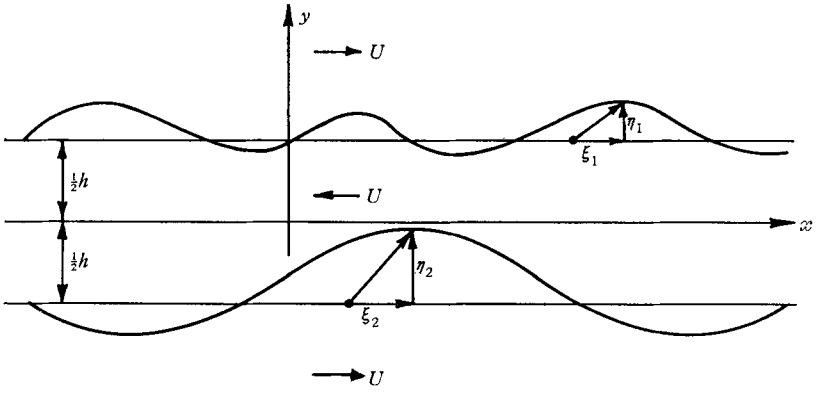

FIGURE 1. A general perturbation of two vortex sheets initially parallel.

respectively of each element of the sheet, originally located at x along the lines $y = \pm \frac{1}{2}h$. Provided that either the Fourier transform or the Fourier series-expansion of the initial disturbance exists, the subsequent linearized history of the system following an arbitrary disturbance can be determined from the response to a disturbance of a particular wavelength.

The problem is to find solutions of Laplace's equation for the velocity potential in all three regions (above, between, and below the sheets) which satisfy the boundary conditions of continuity of pressure and normal component of velocity across each sheet and which imply finite velocity at $y = \pm\infty$ for finite time. The boundary conditions are satisfied only to first order in the displacement of the sheets.

For each wave-number, k, there are necessarily four independent solutions for the velocity potential, each corresponding to a particular mode of displacement of the individual elements of the vortex sheets. These independent modes (called normal modes) can be combined with arbitrary amplitude and phase to satisfy the initial disturbance functions. The normal modes are composed of displacements ξ_1 and η_1 for the upper sheet and ξ_2 and η_2 for the lower sheet:

$$\xi_1 = A\, e^{\nu t} \sin(kx - \omega t), \tag{1}$$

$$\eta_1 = B e^{\nu t} \sin(kx - \omega t), \tag{2}$$

$$\xi_2 = C\, e^{\nu t} \sin(kx - \omega t), \tag{3}$$

$$\eta_2 = D\, e^{\nu t} \sin(kx - \omega t), \tag{4}$$

with the parameters related as shown in table 1.

Modes I and II correspond to symmetric displacements and III and IV to antisymmetric displacements of the individual elements of the vortex sheets. The form of the displacements for each mode is sketched in figure 2. It should be

Mode	ν/k	ω/k	B/A	C/A	D/B
I	$U(1-e^{-2kh})^{\frac{1}{2}}$	$-Ue^{-kh}$	$(\tanh \frac{1}{2}kh)^{\frac{1}{2}}$	$+1$	-1
II	$-U(1-e^{-2kh})^{\frac{1}{2}}$	$-Ue^{-kh}$	$-(\tanh \frac{1}{2}kh)^{\frac{1}{2}}$	$+1$	-1
III	$U(1-e^{-2kh})^{\frac{1}{2}}$	Ue^{-kh}	$(\coth \frac{1}{2}kh)^{\frac{1}{2}}$	-1	$+1$
IV	$-U(1-e^{-2kh})^{\frac{1}{2}}$	Ue^{-kh}	$-(\coth \frac{1}{2}kh)^{\frac{1}{2}}$	-1	$+1$

TABLE 1. The parameters of the normal modes of solution.

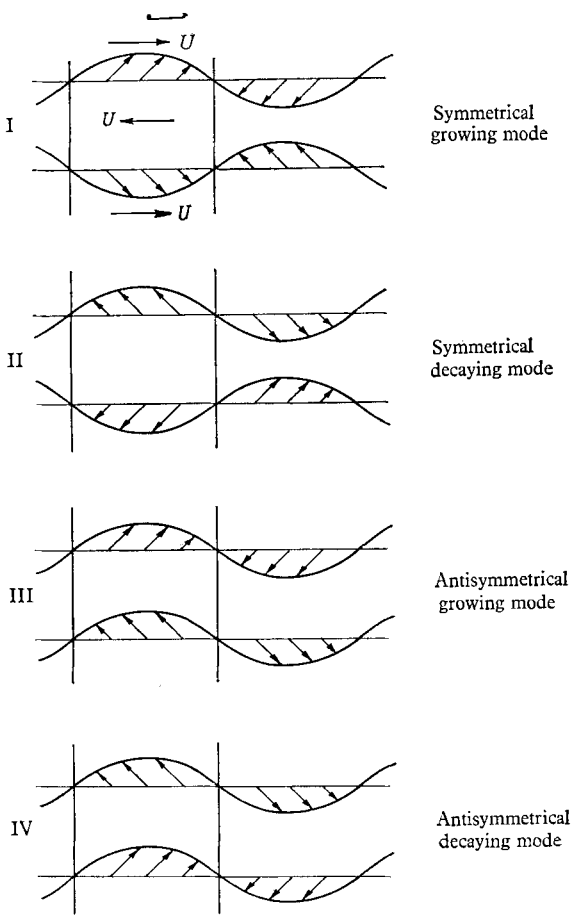

FIGURE 2. A sketch of the four independent periodic modes of a disturbance in two parallel vortex sheets. The displacements of individual elements of the vortex sheets are shown by the arrows.

noted that modes I and III are unstable or growing disturbances, while II and IV are stable or decaying disturbances of the vortex sheets. A pure growing disturbance of the sheets is not simply a vertical displacement of the elements of the vortex sheets, but rather a particular combination of vertical and horizontal displacement. The horizontal displacement leads to a periodic pattern of in-

creasing and decreasing vortex strength along the sheets. The variation of vortex strength in its antisymmetric form (mode III) gives the first indication of a vortex-street arrangement.

The solutions for the initial growth of disturbances in a single sheet of vorticity (often called Helmholtz instability) can be obtained from the results for two sheets (table 1) by simply letting the separation between the sheets, h, approach infinity, giving $\nu = \pm kU$, $\omega = 0$, and $B/A = \pm 1$.

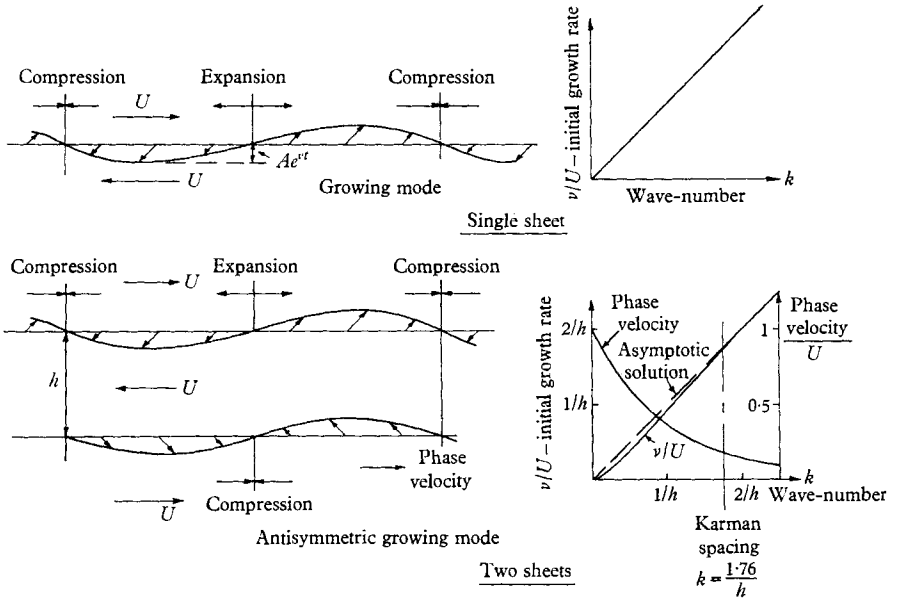

FIGURE 3. A summary of the results of the linear analysis of disturbances in vortex sheets.

The initial growth rate, ν, divided by the reference velocity, U, is plotted against the wave-number, k, in figure 3 for the case of a growing disturbance in a single vortex sheet and an antisymmetric growing disturbance (mode III) in two vortex sheets. The disturbance in the single sheet is a stationary wave, while for the two vortex sheets the disturbance is a travelling wave. The phase velocity (ω/k in table 1) of the antisymmetrical disturbance is also sketched in figure 3.

Since both the symmetrical and antisymmetrical disturbances grow initially at the same rate, no argument based solely on the linearized theory of disturbances of the system can account for the eventual formation of an antisymmetric vortex street. In the Karman idealization of a vortex street, the neutrally stable dimensions of the alternate rows of point vortices was found to be $h/a = 0{\cdot}2805$, with h the distance between rows of vortices a distance a apart. The wave-number, k, corresponding to this spacing ratio is $2\pi(0{\cdot}2805)/h$ or $1{\cdot}76/h$ and is labelled the Karman spacing in figure 3. For such disturbances there is very little interaction in the linearized model between the two vortex sheets. There is a noticeable phase velocity to the disturbance but the growth rate is essentially the same as that for a single sheet. In any case figure 3 discloses that there is nothing in particular about disturbances at the Karman spacing in the linearized model to single them out for special consideration.

4. Non-linear analysis—single sheet

Rosenhead (1931) calculated the early stages of the non-linear growth of an initial periodic disturbance in a vortex sheet assuming that the vortex sheet could be represented by a row of point vortices of finite uniform strength. The initial perturbation of the row of point vortices was simply a small-amplitude sinusoidal displacement of the vortices perpendicular to the line containing the row.† Rosenhead's results (which are sketched in Goldstein 1938, ch. I, § 8) indicated that vortex sheets gradually roll up with the vorticity becoming more and more concentrated in spiral shaped patterns. This suggests a transformation of the infinite vortex sheet into a row of concentrated vortices.

Recently Birkhoff & Fisher (1959) have questioned the notion of smooth rolling-up of a vortex sheet into a row of concentrated vortices. They repeated Rosenhead's calculation using a smaller time step in the integration and more point vortices per wavelength of the initial disturbance and obtained results indicating concentration of vorticity but without smooth roll up. The trajectories they found for the individual vortices in the region of concentration using Rosenhead's initial perturbation, were quite tortuous; smoother paths for the individual point vortices were obtained for normal growing mode initial disturbances (see figure 3).

Birkhoff & Fisher further point out that one cannot expect such a system of point vortices to coalesce into concentrated vortices. They demonstrate in fact that indefinite approach of any pair of point vortices in the system must be accompanied by indefinite recession of other pairs in order for the 'energy' to remain constant.

This criticism of Rosenhead's calculation lead Hama & Burke (1960) to a re-examination of his work. They reproduced Rosenhead's calculations using his time increments and number of vortices per wavelength of disturbance. Decreasing the time increment per step in the numerical calculations while keeping the number of vortices fixed, caused the individual vortex trajectories to become tortuous as Birkhoff & Fisher had found (for a system of more vortices). Again, smoother vortex trajectories were calculated for normal mode initial perturbations.

From these investigations of the growth of disturbances in a single sheet of vorticity one can see a tendency for concentration of vorticity in clouds, but one is cautioned not to expect detail or accurate fine structure within the cloud.

5. Non-linear analysis of antisymmetric disturbances in two vortex sheets

In keeping with § 4 let us first assume that two infinite parallel vortex sheets of constant but opposite strength can be represented by two infinite parallel rows of finite-strength vortices. The vortices in each row are of equal intensity but the sense is opposite in the two rows. Let us now examine the growth of antisym-

† Such a perturbation does not correspond to the pure growing normal mode in figure 3, but represents a disturbance composed of equal amounts of both growing and decaying normal modes of the same amplitude and wavelength.

metrical sinusoidal disturbances of wavelength a in two such rows of vortices initially parallel to the x-axis and a distance h apart (figure 4). The free-stream velocity in the absence of the vortex rows is taken to be U parallel to the x-axis. Let the number of vortex elements per wavelength in each row be n. The strength of the vortices in the upper row is $-2Ua/n$ and in the lower row $2Ua/n$ (positive vorticity counterclockwise). The flow is considered to be inviscid and incompressible.

Following § 3, an antisymmetric sinusoidal disturbance is defined by $\xi_1(x) = -\xi_2(x)$ and $\eta_1(x) = \eta_2(x)$. If the wavelength of the disturbance is a, this definition is equivalent to $\xi_1(x) = \xi_2(x+\frac{1}{2}a)$ and $\eta_1(x) = -\eta_2(x+\frac{1}{2}a)$. Hence this antisymmetric disturbance may also be described as shifted-symmetric (a symmetric disturbance shifted by one half-wavelength in one sheet); this equivalence holds only for sinusoidal disturbances, and the appropriate restriction on the configuration of the vortex rows in the non-linear stages of growth is that of shifted-symmetry rather than antisymmetry.

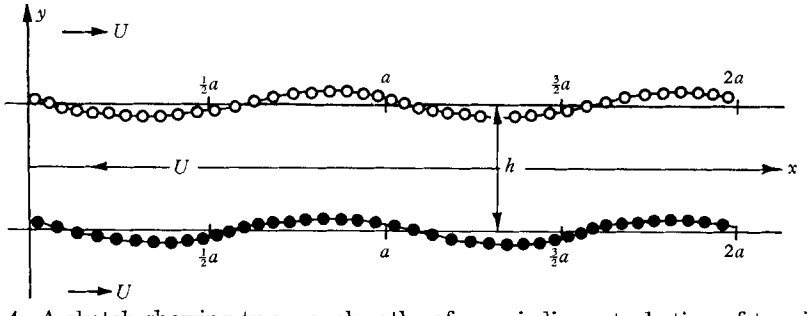

FIGURE 4. A sketch showing two wavelengths of a periodic perturbation of two initially parallel infinite vortex rows. ○, Vortex element with clockwise rotation; ●, vortex element with counterclockwise rotation.

Let the co-ordinates of the ith vortex element in the upper row of vortices be $x_i(t)$, $y_i(t)$ at time t, and let the horizontal and vertical components of the velocity of this element induced by all other vortex elements and the free-stream motion be $u_i(t)$ and $v_i(t)$ respectively. Since this analysis is restricted to shifted-symmetric periodic disturbances, the ith vortex element in the lower row corresponds in position to an element which is one half-wavelength advanced from the ith vortex element in the upper row. Then

$$x_i(t) + \tfrac{1}{2}a = x_i^l(t) \quad (i = 1, 2, \ldots, n), \tag{5}$$

$$y_i(t) = -y_i^l(t) \quad (i = 1, 2, \ldots, n), \tag{6}$$

where the superscript l signifies the lower row.

Differentiation of (5) and (6) with respect to time gives

$$u_i(t) = u_i^l(t), \tag{7}$$

$$v_i(t) = -v_i^l(t), \tag{8}$$

the relationship between the velocity components of corresponding vortex elements in the upper and lower rows.

The differential equations which govern the motion of the vortices may be written

$$dx_i/dt = u_i(x_1, x_2, \ldots, x_n, y_1, y_2, \ldots, y_n), \tag{9}$$

$$dy_i/dt = v_i(x_1, x_2, \ldots, x_n, y_1, y_2, \ldots, y_n), \tag{10}$$

in which u_i and v_i can be considered to be known functions of position in the differential equations. It is not necessary to calculate x_i^l and y_i^l explicitly since they are uniquely related to x_i and y_i by (5) and (6); however, in calculating u_i and v_i the influence of the lower row of vortices on the upper row must be considered.

The velocity components u_i and v_i can be determined by considering the velocity induced at the location of the ith vortex by all other vortices of the system and by the free-stream motion. The periodic arrangement of n vortices per wavelength, a, in the upper and lower rows can be thought of as composed of n separate sub-arrangements of vortices. Each sub-arrangement for a given row is composed of an infinite row of vortices of strength $\pm 2Ua/n$ located a distance a apart and parallel to the x-axis (see figure 4). The components of the velocity induced at (x_i, y_i) due to such a sub-arrangement of vortices of the upper row with coordinates

$$(x_j, y_j),\ (x_j \pm a, y_j),\ (x_j \pm 2a, y_j), \ldots$$

are (see Lamb 1932, § 156)

$$u_{ij} = \frac{U}{n}\left[\frac{\sinh 2\pi(y_i - y_j)/a}{\cosh 2\pi(y_i - y_j)/a - \cos 2\pi(x_i - x_j)/a}\right], \tag{11}$$

$$v_{ij} = -\frac{U}{n}\left[\frac{\sin 2\pi(x_i - x_j)/a}{\cosh 2\pi(y_i - y_j)/a - \cos 2\pi(x_i - x_j)/a}\right]. \tag{12}$$

Similarly, the velocity components u'_{ij} and v'_{ij} at (x_i, y_i) due to such a sub-arrangement of vortices of strength $2Ua/n$ with coordinates

$$(x_j^l, y_j^l),\quad (x_j^l \pm a, y_j^l),\quad (x_j^l \pm 2a, y_j^l),\quad \ldots$$

are

$$u'_{ij} = -\frac{U}{n}\left[\frac{\sinh 2\pi(y_i + y_j)/a}{\cosh 2\pi(y_i + y_j)/a + \cos 2\pi(x_i - x_j)/a}\right], \tag{13}$$

$$v'_{ij} = -\frac{U}{n}\left[\frac{\sin 2\pi(x_i - x_j)/a}{\cosh 2\pi(y_i + y_j)/a + \cos 2\pi(x_i - x_j)/a}\right], \tag{14}$$

in which the coordinates x_j^l and y_j^l have been expressed in terms of x_j and y_j by using (5) and (6).

The velocity of an individual vortex element located at (x_i, y_i) is composed of the horizontal component U due to the free-stream motion and the induced velocity due to all other vortex elements; therefore,

$$u_i = U + \sum_{j=1}^{n} (u_{ij} + u'_{ij}), \tag{15}$$

$$v_i = \sum_{j=1}^{n} (v_{ij} + v'_{ij}). \tag{16}$$

The mean horizontal velocity of translation of the vortex system, $\overline{U}$, is simply the average value of u_i for all of the vortices in a wavelength, or

$$\overline{U} = \frac{1}{n}\sum_{i=1}^{n} u_i = U + \frac{1}{n}\sum_{i=1}^{n}\sum_{j=1}^{n} (u_{ij} + u'_{ij}). \tag{17}$$

By noting that u_{ij} is antisymmetric in i and j (and that therefore its double summation on i and j is identically zero) $\overline{U}$ can be simply expressed as

$$\overline{U} = U + \frac{1}{n} \sum_{i=1}^{n} \sum_{j=1}^{n} u'_{ij}, \tag{18}$$

which indicates that the mean translational velocity of the upper row is entirely due to the vortices in the lower row (and vice versa) even when the row is distorted,† i.e. when $y_i \neq \frac{1}{2}h$ for all i. The mean vertical velocity, $\overline{V}$, of the vortices in the upper row, averaged over a wavelength, is simply,

$$\overline{V} = \frac{1}{n} \sum_{i=1}^{n} v_i = \frac{1}{n} \sum_{i=1}^{n} \sum_{j=1}^{n} (v_{ij} + v'_{ij}). \tag{19}$$

Since both v_{ij} and v'_{ij} are antisymmetric in i and j the double summations are identically zero, and (19) becomes

$$\overline{V} \equiv 0, \quad t \geqslant 0 \tag{20}$$

(for all values of time). Equation (20) immediately implies that the average vertical displacement of all the elements in either the upper or lower rows is zero for all values of time.

The differential equations (9) and (10) for the position of the vortices in the upper row can now be solved as a function of time. Unfortunately the velocity components, (15) and (16), are non-linear functions of position of the vortices, necessitating a numerical solution of the differential equations.

The basic procedure used in the solution was straightforward. For a given configuration of the vortices, u_i and v_i were computed for all vortices

$$(i = 1, 2, \ldots, n);$$

these computed velocity components for each vortex were then modified, on the basis of the past velocities of each vortex, to give an average value of velocity for a time increment Δt. Based on the calculated average velocity and Δt, a new position was determined for each vortex; u_i and v_i were then recalculated for the new configuration and the process repeated. The number of individual calculations involved in integrating (15) and (16) in this manner is so large that the calculations were, by necessity, performed on a high-speed electronic digital computer. The actual integrating programme employed was the SHARE–program GL–AIDE. The time step, Δt, in the integrations was varied from $0{\cdot}002a/U$ to $0{\cdot}02a/U$, with the majority of the runs calculated with $\Delta t = 0{\cdot}004a/U$. Halving the time step from this value did not noticeably affect the results. Most of the calculations were performed with 21 vortices per wavelength in each row. While one would have liked to have had more vortices per wavelength in order to increase the detail in the results, it was found that roughly 20 vortices per wavelength represented a reasonable compromise between detail and the expense

† In the undisturbed configuration the vortex rows are not exactly at rest in the coordinate system shown in figure 4, but move in the x-direction with a velocity

$$= U\{1 - [\coth(\pi nh/a)]^{(-1)^n}\}.$$

For the values of $\pi nh/a$ to be considered here, the velocity of the undisturbed vortex system is very small.

of the machine calculations (doubling n increases the calculation time by a factor of four). The number 21 rather than 20 for n was decided on the basis of preliminary runs which will be discussed later. Given the time step in the integration, Δt, and the number of vortices, the parameters to be investigated are simply the spacing ratio, h/a, and the form of the initial shifted-symmetrical disturbance of the vortices.

If Δx_i and Δy_i are the horizontal and vertical displacements of the ith vortex in the upper row due to the initial perturbation, then $x_i(0), y_i(0)$, the co-ordinates of the ith vortex after the perturbation, are

$$x_i(0) = (i-1)\,a/n + \Delta x_i \quad (i = 1, 2, \ldots, n); \tag{21}$$

$$y_i(0) = \tfrac{1}{2}h + \Delta y_i \quad (i = 1, 2, \ldots, n). \tag{22}$$

The undisturbed co-ordinates of the ith vortex in the upper row are $(i-1)\,a/n, \frac{1}{2}h$; time, t, has been taken to be zero at the initial perturbation. Equations (21) and (22) can be expressed in terms of (1) and (2) as

$$x_i(0) = \frac{(i-1)\,a}{n} + A \sin \frac{2\pi(i-1)}{n} \quad (i = 1, 2, \ldots, n); \tag{23}$$

$$y_i(0) = \tfrac{1}{2}h + B \sin \frac{2\pi(i-1)}{n} \quad (i = 1, 2, \ldots, n). \tag{24}$$

From § 3 it is known that there are two normal modes of small-amplitude disturbances (modes III and IV of table 1) which are specified by the ratio of B to A. For values of B/A other than those of table 1, the perturbation is simply a linear combination of the two pure modes. If (24) is rewritten as

$$y_i(0) = \tfrac{1}{2}h + \gamma A \sin \frac{2\pi(i-1)}{n} \quad (i = 1, 2, \ldots, n), \tag{25}$$

then one can think of A as the size of the perturbation and γ as the ratio of B/A in (23) and (24). The value of γ determines the combination of pure modes in the initial disturbance. If A_{III} and A_{IV} are sizes of the growing and decaying modes respectively, then the ratios of A_{III} and A_{IV} to A (A is the size of the total disturbance) are expressed in terms of γ as

$$\frac{A_{\mathrm{III}}}{A} = \frac{(\coth \pi h/a)^{\frac{1}{2}} + \gamma}{2(\coth \pi h/a)^{\frac{1}{2}}}, \quad \frac{A_{\mathrm{IV}}}{A} = \frac{(\coth \pi h/a)^{\frac{1}{2}} - \gamma}{2(\coth \pi h/a)^{\frac{1}{2}}}. \tag{26}$$

While Birkhoff & Fisher (1959) and Hama & Burke (1960) found, for a single row of vortices, that a pure growing-mode perturbation was necessary in order to have smooth paths for subsequent motions of the vortices, no such restriction was found to be necessary in the problem being considered. Therefore all but one of the calculations presented here have an initial disturbance composed of both growing and decaying modes, the amount of each present in the perturbation depending on γ.†

† An initial perturbation which is not purely a growing or decaying mode actually represents a large class of known initial conditions provided the amplitude is small enough for the linearized theory of § 3 to be valid. Consider a given perturbation of the form of (23) and (25) with γ and A fixed. In a small amount of time, $\pm\tau$, the original perturbation would change to new configurations determined by (1) and (2). These new configurations could just as well be considered the initial disturbance as the original perturbation.

The results of the calculations of the positions of the vortices at various times after the initial disturbance, for particular values of h/a, have been plotted in figures 5 to 14. The individual drawings in these figures show the stages in the development of vortex streets. The solid lines in the sketches, which connect the individual vortices consecutively on the basis of their relative positions in the undisturbed vortex rows, were drawn in to suggest a continuous vortex sheet.

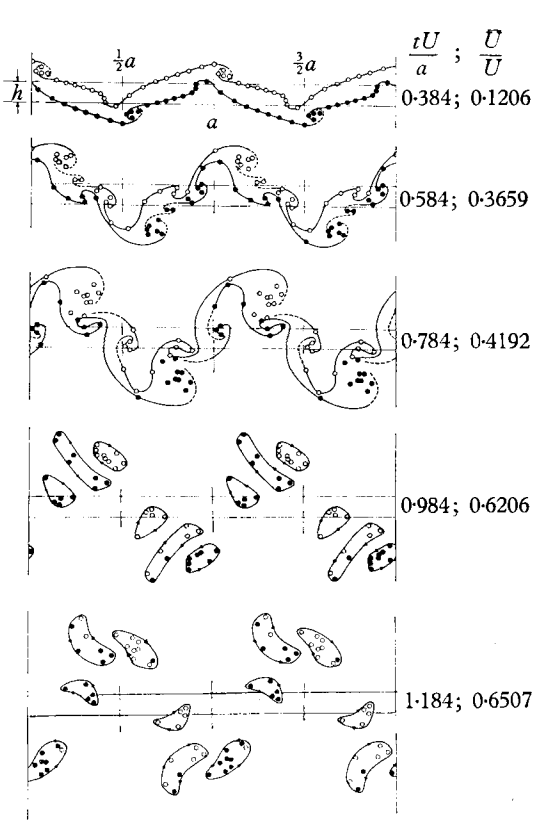

FIGURE 5

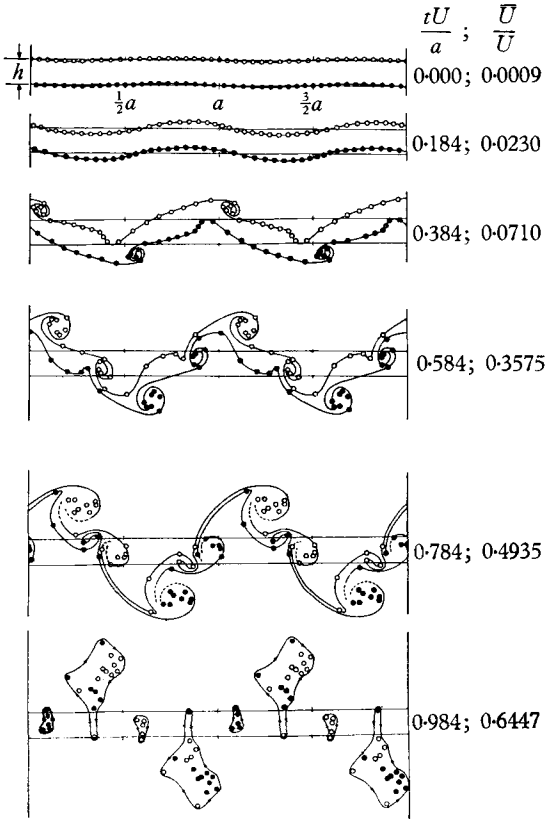

FIGURE 6

FIGURE 5. Vortex street formation with $h/a = 0{\cdot}120$, $A = -0{\cdot}0125a$, $\gamma = (\tanh \pi h/a)^{\frac{1}{2}}$, $n = 21$, and $\Delta t = 0{\cdot}004a/U$.

FIGURE 6. Vortex street formation with $h/a = 0{\cdot}140$, $A = -0{\cdot}0125a$, $\gamma = (\tanh \pi h/a)^{\frac{1}{2}}$, $n = 21$, and $\Delta t = 0{\cdot}004a/U$.

A line was not drawn connecting the vortices within the regions of vortex concentration, since such a suggestion of fine structure of continuous vorticity within the clouds seemed unjustified, owing to the discrete distribution of vorticity used in the calculations. On the basis of the location of the last vortex to be swept into the cloud, a dotted line was generally drawn in connecting the clouds to the solid curves. In the last stages of the development of the vortex streets, the concentration of vortices into individual clouds had progressed to such an extent that there was no longer sufficient evidence to suggest the existence of vortex sheets. Instead a solid line was simply drawn surrounding the individual clouds with

arrowheads indicating the sense of rotation of the net vorticity within the individual clouds.

The spacing ratio (h/a), A and γ of the original perturbation, the number of vortices per wavelength in each row (n), and the time increment (Δt) in the integration for each vortex system are given in the captions of the figures. The elapsed time in the integration from the original perturbation to each later

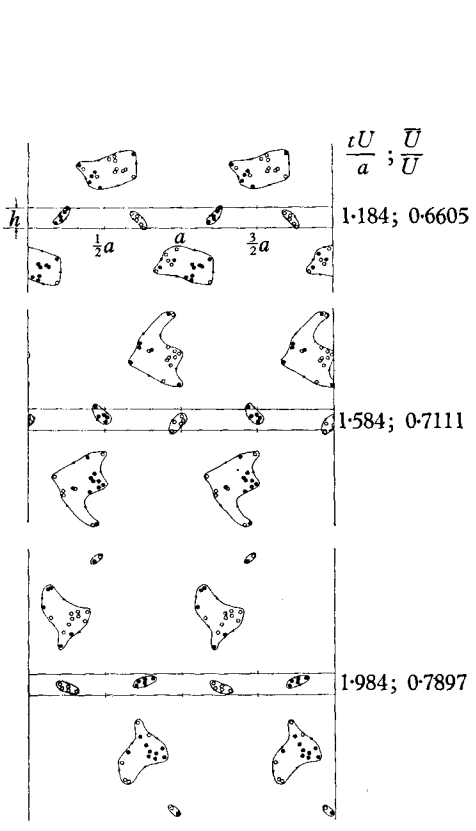

FIGURE 7

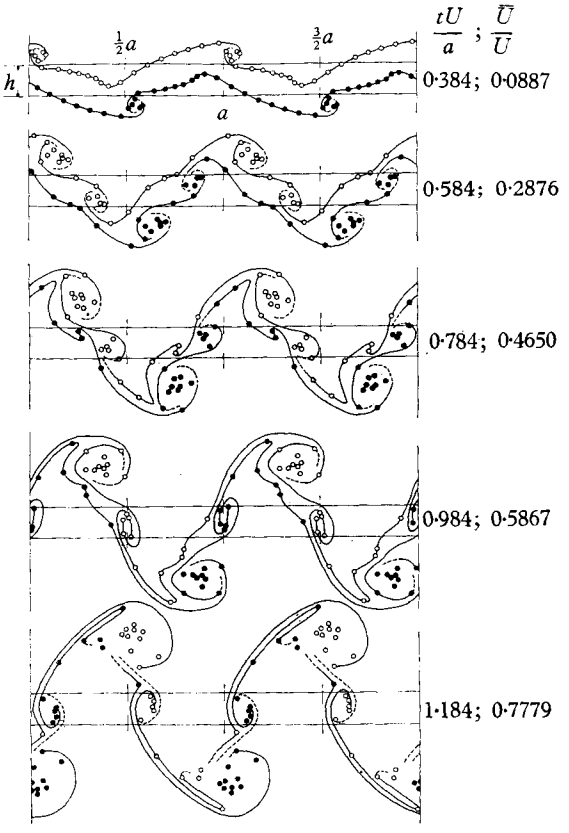

FIGURE 8

FIGURE 7. Later stages of the development of the vortex street system of figure 6.

FIGURE 8. Vortex street formation with $h/a = 0{\cdot}170$, $A = -0{\cdot}0125a$, $\gamma = (\tanh \pi h/a)^{\frac{1}{2}}$, $n = 21$, and $\Delta t = 0{\cdot}004a/U$.

configuration sketched is shown immediately to the right of each drawing along with the value of $\bar{U}/U$ for that configuration. The open and solid circles in the drawings represent vortices with clockwise and counterclockwise senses of rotation respectively. The wavelength, a, in all sketches is the same; h varies to give the appropriate value of h/a. Parallel lines denoting the original separation between undisturbed rows of vortices are shown in all sketches. The calculated values of $\bar{U}/U$ are plotted in figures 15 and 16 as a function of time for all of the vortex systems investigated. Figures 5 to 13 are numbered in order of increasing value of h/a.

6. Discussion of results

There appears to be a fairly general pattern followed in the formation of vortex streets from vortex rows, which is independent of h/a. In the early stages (see, for example, the second sketch of figure 6 or the first sketch of figure 10), the shifted-symmetrical disturbance grows in a manner similar to that predicted by the linearized theory of § 3. Rolling up or concentration of the vortices can be

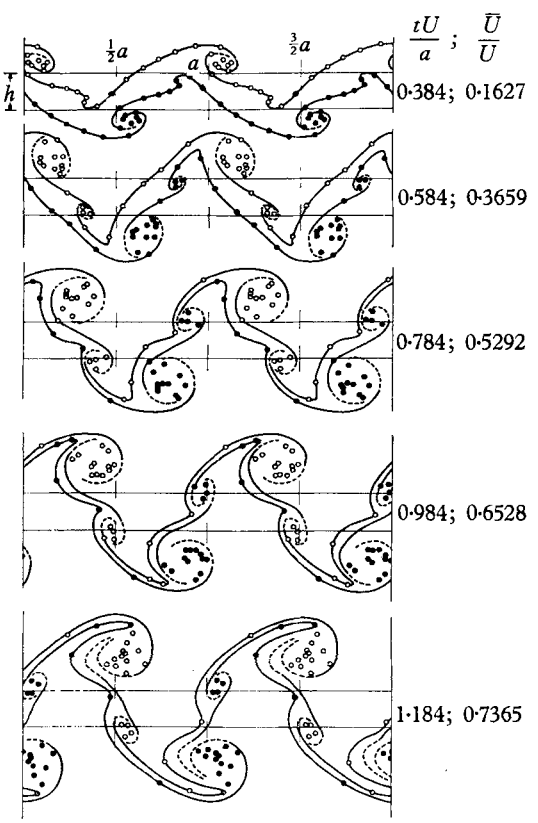

FIGURE 9

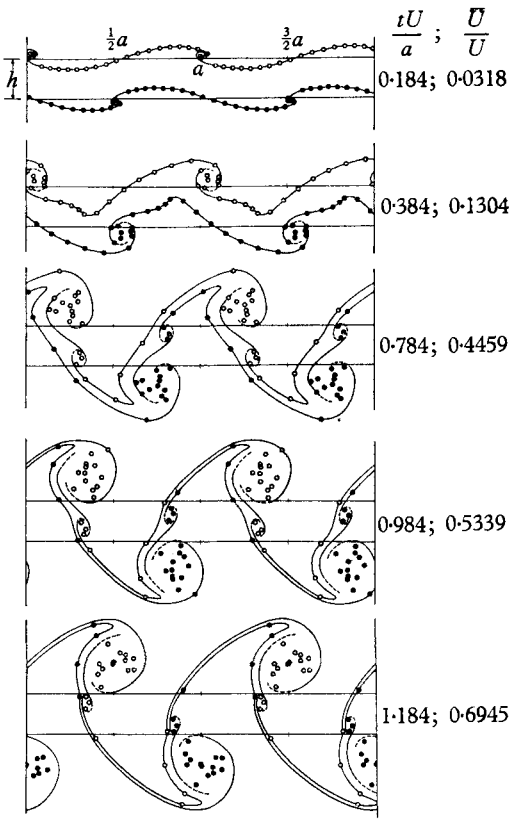

FIGURE 10

FIGURE 9. Vortex street formation with $h/a = 0{\cdot}210$, $A = -0{\cdot}0250a$, $\gamma = (\tanh \pi h/a)^{\frac{1}{2}}$, $n = 21$, and $\Delta t = 0{\cdot}004a/U$.

FIGURE 10. Vortex street formation with $h/a = 0{\cdot}240$, $A = -0{\cdot}0250a$, $\gamma = (\tanh \pi h/a)^{\frac{1}{2}}$, $n = 21$, and $\Delta t = 0{\cdot}004a/U$.

seen near $x = 0, a, 2a$ in the upper row and near $x = \frac{1}{2}a, \frac{3}{2}a$ in the lower row. This early stage is characterized by negligible interaction between the vortex rows.

The intermediate stage of the development, on the other hand, is dominated by the interaction of the two vortex rows. As the concentration of vortices and the growth of the transverse displacement of the vortices in the early stage proceeds, the vortices displaced from one row toward the other row tend to be swept into the outer mantle of the cloud of vortices forming in the other row. The last four sketches of figure 10 are typical illustrations of the intermediate

stage of vortex street development. The mutual interaction in this stage of the development between the portions of each vortex row which are swept toward the opposite row is a function of h/a, decreasing with increasing values of h/a. The final stage of vortex street formation is the concentration of all individual vortices into clouds of vorticity or eddies. It is presumed that if viscosity were present its major effect on the vortex street formation would be to effect cancel-

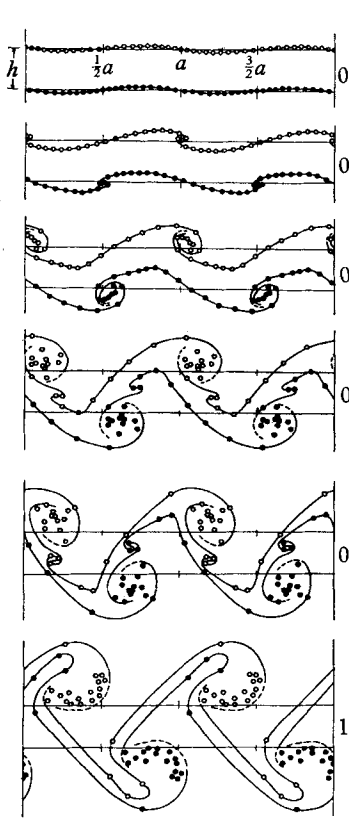

FIGURE 11

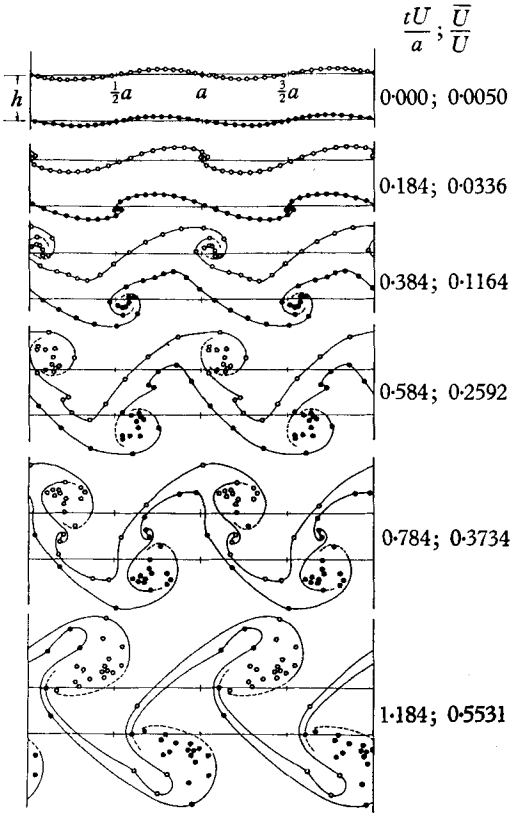

FIGURE 12

FIGURE 11. Vortex street formation with $h/a = 0{\cdot}281$, $A = -0{\cdot}0250a$, $\gamma = (\tanh \pi h/a)^{\frac{1}{2}}$, $n = 21$, and $\Delta t = 0{\cdot}004a/U$.

FIGURE 12. Vortex street formation with $h/a = 0{\cdot}281$, $A = -0{\cdot}0250a$, $\gamma = (\coth \pi h/a)^{\frac{1}{2}}$, $n = 21$, and $\Delta t = 0{\cdot}004a/U$.

lation of vorticity of opposite sign by diffusion within the clouds formed in this final stage.

The value of h/a of the system does not alter the general pattern of vortex street formation but rather influences the details of the interactions. In general, increasing the value of h/a (1) decreases the number of individual clouds of vorticity formed per wavelength, (2) increases the net vorticity in the outer vortex clouds, and (3) increases the time required to reach the final stage of development. The details of the dependence of the interaction on h/a can be seen by comparing figures 5 through 13.

In the intermediate stage of development there exists what might be called a competition between two separate mechanisms of interaction of the original vortex rows. At the larger values of h/a, portions of each vortex row are swept across to the vortex clouds forming on the opposite side (see figure 13). At the smaller values of h/a these portions of the vortex rows start out for the other side

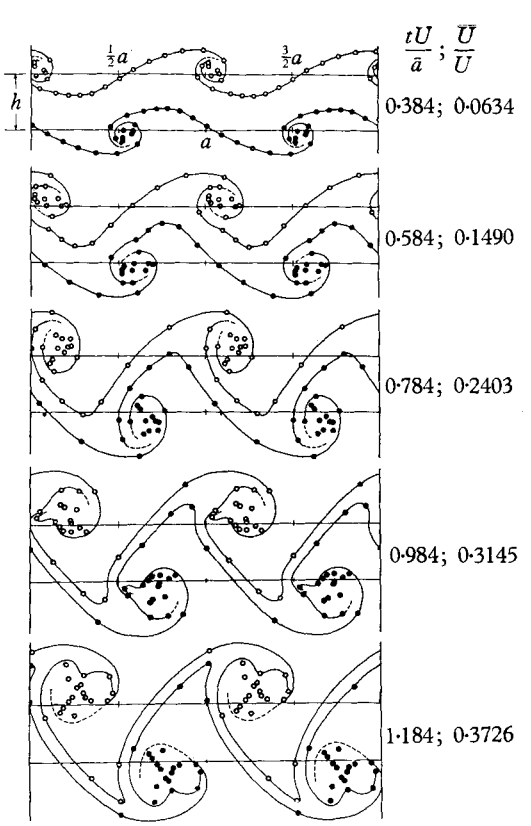

FIGURE 13

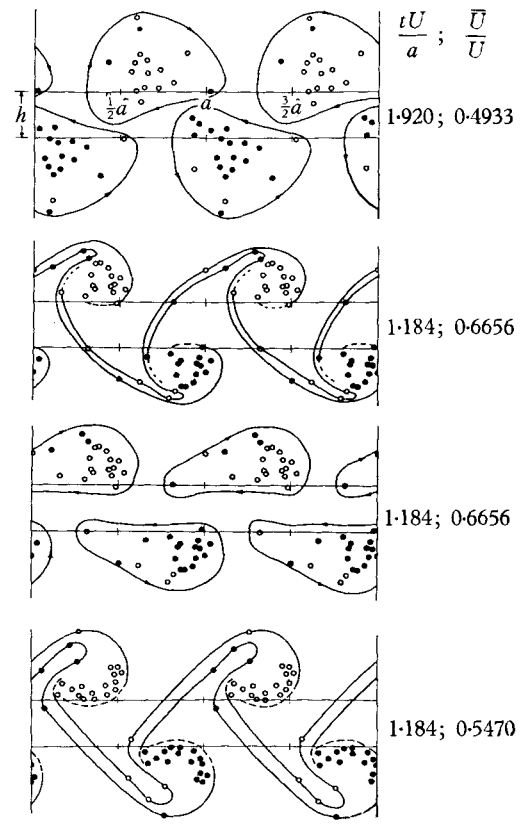

FIGURE 14

FIGURE 13. Vortex street formation with $h/a = 0{\cdot}340$, $A = -0{\cdot}0250a$, $\gamma = (\tanh \pi h/a)^{\frac{1}{2}}$, $n = 21$, and $\Delta t = 0{\cdot}004a/U$.

FIGURE 14. From the top down. First sketch: vortex street formed with $h/a = 0{\cdot}281$, small initial perturbation with short-wavelength components, $n = 20$, $\Delta t = 0{\cdot}02a/U$. Second sketch: vortex street formed with $h/a = 0{\cdot}281$, $A = -0{\cdot}0250a$, $\gamma = (\tanh \pi h/a)^{\frac{1}{2}}$, $n = 20$, and $\Delta t = 0{\cdot}004a/U$. Third sketch: the same system as the second sketch with boundaries of vortex clouds drawn rather than continuous vortex sheets. Fourth sketch: vortex street formed with $h/a = 0{\cdot}281$, $A = -0{\cdot}0250a$, $\gamma = (\tanh \pi h/a)^{\frac{1}{2}}$, $n = 21$, and $\Delta t = 0{\cdot}004a/U$.

but before they reach it they concentrate to form separate vortex clouds as shown in figure 5. For values of h/a between these two extremes, parts of both mechanisms of interaction exist; some vortices are swept across to the outer clouds and others form smaller clouds between them. Increasing h/a decreases the strength of these inner clouds. The numbers of individual vortex clouds formed and their net strength as a function of h/a are summarized in table 2. The net strength of a cloud is simply the number of vortices in the cloud, after allowing

for cancellation of equal numbers of positive and negative elements. All of the systems of figures 5 to 13, on which table 2 is based, have $n = 21$.

Note that $h/a = 0{\cdot}28$ is the smallest sheet spacing investigated for which only two clouds form per wavelength, while $h/a = 0{\cdot}14$ is the smallest sheet spacing for which only four clouds form per wavelength. Furthermore, $h/a = 0{\cdot}14$ or $0{\cdot}17$ are the spacings for which all four clouds are of approximately equal strength. This suggests that the Karman spacing ratio of 0·28 has a special importance quite independent of the stability analysis from which it was derived and which has been subjected to steady criticism. That is, the number of equal strength vortex clouds per half wavelength times the original spacing ratio is (approximately) the ratio 0·28. One is tempted to expect this pattern to persist even for smaller h/a than studied here and for a wider variety of initial conditions.

h/a	No. of vortex clouds formed per wavelength	Net strength of clouds	
		Outer	Inner
0·12	6	7	3; 5
0·14	4	4	5
0·17	4	5	4
0·21	4	9	4
0·24	4	10	3
0·28	2	13	—
0·34	2	15	—

TABLE 2. Summary of vortex cloud formations.

Figures 11 and 12 show the development of vortex streets for similar systems with different initial conditions. The system shown in figure 12 was perturbed with a growing mode alone while mixed growing and decaying modes were used in the system of figure 11. The differences between the two systems at like values of tU/a are exceedingly small and suggest relative insensitivity to the form of the initial perturbation.

Figure 14 presents a comparison between a number of systems. The first sketch shows a vortex system for which $n = 20$ and $\Delta t = 0{\cdot}020$, five times the increment used in all other calculations. The amplitude of the initial perturbation was small and contained short-wavelength components. The final stage in the development was rapidly reached, the interaction was haphazard, but the final stage is similar to the one shown in the third sketch for which the initial perturbation was smoother and Δt much smaller. The second and third sketches are of the same vortex system; the difference lies in what might be called the authors' artistic interpretation of the results. The lines in the second sketch suggest continuous vortex sheets while the same system (the location of the individual vortices in the two sketches is exactly the same) is viewed in the third sketch as though the vortices were already concentrated in clouds. The last sketch in figure 14 and the second compare systems with different values of n; the two are quite similar. When the calculations for the second sketch were carried further in time, the last vortex of the tails being swept into the clouds never managed to enter the clouds

but began to wander to the left between the outer clouds. When n was increased to 21 (last sketch of the figure) this did not happen. It was because of this that $n = 21$ was initially selected for all of the other calculations. The differences among the various vortex systems can also be seen from the plots of $\bar{U}/U$ in figures 15 and 16.

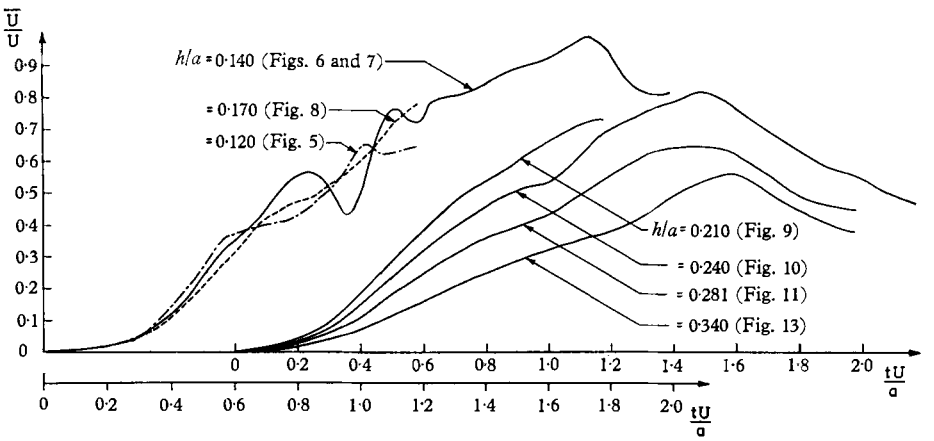

FIGURE 15. A plot of the calculated average velocity of various vortex systems as a function of time. The details of each system are given in the captions of the indicated figures.

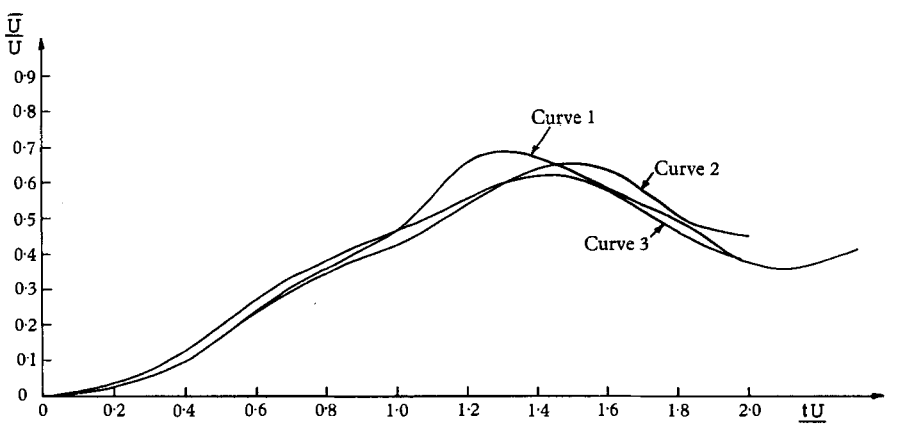

FIGURE 16. A comparison of calculated average velocity of vortex systems with $h/a = 0{\cdot}281$ and $\Delta t = 0{\cdot}004a/U$, but with different initial conditions or number of vortices per wavelength. Curve 1: $A = -0{\cdot}0250a$, $\gamma = (\tanh \pi h/a)^{\frac{1}{2}}$, $n = 20$. Curve 2: $A = -0{\cdot}0250a$, $\gamma = (\tanh \pi h/a)^{\frac{1}{2}}$, $n = 21$. Curve 3: $A = -0{\cdot}0250a$, $\gamma = (\coth \pi h/a)^{\frac{1}{2}}$, $n = 21$.

There are two important observed features of vortex street formation which are explained by the results of § 5, namely: (1) broadening of the vortex street with the distance downstream in the wake, and (2) cancellation of part of the vorticity discharged from the body in the formation of the vortex street. These features, which were thought to be separate, are actually intimately connected; the broadening following of necessity from the vortex cancellation. The broadening of the vortex street with distance downstream in the wake is clearly shown in the

photographs of actual street formation taken by Homann (see Goldstein 1936, ch. 13, § 240) and in all of the calculated results of § 5. Consider for example the sketches of figure 11 for which $h/a = 0{\cdot}28$, the value of the observed spacing ratio near a bluff body. If one interchanges time with downstream position in the wake, then the composite picture of street formation obtained in this way agrees remarkably well with Homann's photographs. As portions of vorticity from one side are swept across to the other side the remaining vorticity must move away from the opposite side because from equation (20) the average transverse displacement of the vortex row must be zero. The explanation of vortex street broadening is as simple as that. The vorticity which is swept from one side to the other, decreases the net strength of the vortex cloud formed primarily of vorticity of the opposite sense.

Once the interaction between the vortex rows has progressed to the stage of forming distinct clouds of vorticity, the vortex street has essentially been formed. Further broadening of the street in an inviscid fluid is impossible. In a corollary to their momentum invariance theorem, Birkhoff & Zarantonello (1957, ch. 13, § 6) show that the broadening of an infinite street of equal strength and alternate sense eddies is possible only in viscous plane flow.

In the last sketch of figure 11, the four vortices comprising the tails of vorticity of opposite sign being swept into the clouds reduce the net strength of the clouds to that of 13 individual vortices. Without interaction between the rows the strength of the clouds would have been 21 (the value of n); hence the interaction of the vortex rows reduces the strength of the clouds to $\frac{13}{21}$ or roughly 60 % of the total strength of the original vortex rows per wavelength. This is exactly the value of the strength of eddies reported by Fage & Johansen (1927) and discussed in § 1 of this paper.

Within these large eddies the vortex elements of opposite sense are not randomly distributed but rather form an outer mantle. Therefore the initial action of viscosity would be to cause cancellation in this outer mantle alone, leaving the core well defined. This undoubtedly explains the persistence of recognizable eddies far downstream from the body, even when the eddies are turbulent.

The actual spacing ratio of the vortex street far downstream in the wake of a cylinder (i.e. sufficiently far downstream for the concentration of vorticity to be essentially completed) can be estimated to be 0·5 from Homann's photograph for a Reynolds number of 101. The spacing ratio of the calculated vortex street in figure 11 is also roughly 0·5. It is difficult to measure the spacing ratio either from actual photographs of vortex streets or from the computed streets because of the uncertainty in locating the centre of the large diffuse eddies which make up the street. In the process of forming these large eddies, all the fluid originally between the parallel vortex sheets remains trapped between them and so is swept into the eddies. Some fluid outside the sheets is also swept in, and therefore the area of the fully developed eddies will be larger than that of the wake from which they are formed.

7. Conclusions

The essential features of the formation of vortex streets from the vortex layers emanating from bluff bodies can be explained simply by the growth of disturbances in two infinite, initially parallel, vortex rows in an inviscid incompressible fluid. A linearized analysis of the growth of disturbances does indicate regions of concentration of vorticity along the vortex sheets, but does not indicate strong interaction between the vortex sheets for the spacing ratios of disturbances of interest. The important features of vortex street formation can only be elucidated by considering the growth of large amplitude disturbances. The observed broadening of vortex streets downstream in the wakes of bluff bodies is a direct consequence of the interaction of the vortex rows. This interaction leads to the formation of concentrated clouds of vorticity with a net strength diminished by the vorticity swept into the cloud from the opposite vortex row.

The machine programming and calculations for the work presented in this paper were supported by the Office of Naval Research under contracts NONR 1866–20 and NONR 1866–34. A grant from the Joseph Clark Bequest of Harvard University made possible the preparation of the figures.

We are indebted to Steven R. Russell of the Littauer Statistical Laboratory for assistance in the programming of the calculations.

REFERENCES

BIRKHOFF, G. & ZARANTONELLO, E. H. 1957 *Jets, Wakes, and Cavities.* New York: Academic Press.

BIRKHOFF, G. & FISHER, J. 1959 Do vortex sheets roll up? *Rendi. Circ. Mat. Palermo,* Ser. 2, **8**, 77–90.

FAGE, A. & JOHANSEN, F. C. 1927 On the flow of air behind an inclined flat plate of infinite span. *Proc. Roy. Soc.* A, **116**, 170–97.

FAGE, A. & JOHANSEN, F. C. 1928 The structure of the vortex sheet. *Phil. Mag.* **5**, 417–41.

GOLDSTEIN, S. (ed.) 1938 *Modern Developments in Fluid Dynamics.* Oxford: The Clarendon Press.

HAMA, F. R. & BURKE, E. R. 1960 On the rolling-up of a vortex sheet. *Univ. of Maryland, Tech. Note* no. BN-220.

HOMANN, F. 1936 Einfluss grosser Zähigheit bei Strömung um Zylinder. *Forschung auf dem Gebiete des Ingenieurwesens,* **7**, 1–10.

KARMAN, TH. VON 1911 Über den Mechanismus des Widerstandes, den ein bewegter Körper in einer Flüssigkeit erfährt. *Gottinger Nachrichten, math.-phys. Kl.* pp. 509–17.

KOVASZNAY, L. S. G. 1949 Hot-wire investigation of the wake behind cylinders at low Reynolds numbers. *Proc. Roy. Soc.* A, **198**, 174–90.

LAMB, H. 1932 *Hydrodynamics,* 6th ed. Cambridge University Press.

LIPPISCH, A. M. 1958 Flow visualization. *Aero. Eng. Rev.* **17**, 24–32.

RAYLEIGH, LORD 1894 *The Theory of Sound,* vol. II. Cambridge University Press. (Reprinted 1945, New York: Dover).

ROSENHEAD, L. 1931 The formation of vortices from a surface of discontinuity. *Proc. Roy. Soc.* A, **134**, 170–92.

ROSHKO, A. 1954*a* On the development of turbulent wakes from vortex streets. *Nat. Adv. Comm. Aero., Wash., Rep.* no. 1191.

ROSHKO, A. 1954*b* On the drag and shedding frequency of bluff cylinders. *Nat. Adv. Comm. Aero., Wash., Tech. Note* no. 3169.